Nanoscale

# Surface Modification Nanoarchitectonics of Carbon Nitride Dots for Better Drug Loading and Higher Cancer Selectivity



| | |
|---|---|
| Journal: | *Nanoscale* |
| Manuscript ID | NR-ART-04-2022-002063.R1 |
| Article Type: | Paper |
| Date Submitted by the Author: | 27-May-2022 |





| | |
|---|---|
| Complete List of Authors: | Leblanc, Roger; University of Miami, Department of Chemistry<br>Kirbas, Emel; University of Miami, Department of Chemistry<br>Sankaran, Meghana; University of Miami Miller School of Medicine, Department of Neurosurgery<br>Garber, Jordan ; University of Miami, Department of Chemistry<br>Vallejo, Frederic ; University of Miami Miller School of Medicine, Department of Neurosurgery<br>Bartoli, Mattia; Polytechnic of Turin, DISAT<br>Tagliaferro, Alberto; Politecnico di Torino, DISAT; University of Ontario Institute of Technology,<br>Vanni, Steven; University of Miami School of Medicine, Department of Neurological Surgery<br>Graham, Regina; University of Miami School of Medicine, Department of Neurological Surgery |
| | |

# Surface Modification Nanoarchitectonics of Carbon Nitride Dots for Better Drug Loading and Higher Cancer Selectivity

Emel Kirbas Cilingir [a], Meghana Sankaran [b], Jordan M. Garber [a], Frederic Anthony Vallejo [b, c], Mattia Bartoli [d], Alberto Tagliaferro [d], Steven Vanni [b, e, f], Regina M. Graham [b, c, g*] and Roger M. Leblanc [a*]

[a] *Department of Chemistry, University of Miami, 1301 Memorial Drive, Coral Gables, Florida 33146, United States.*

[b] *Department of Neurosurgery, University of Miami Miller School of Medicine, 1095 NW 14th Terrace, Miami, FL 33136, USA*

[c] *University of Miami Brain Tumor Initiative, Department of Neurosurgery, University of Miami Miller School of Medicine, 1095 NW 14th Terrace, Miami, FL 33136, USA*

[d] *Department of Applied Science and Technology, Politecnico di Torino, Italy*

[e] *HCA Florida University Hospital, 3476 S University Dr., Davie, FL 33328*

[f] *Dr. Kiran C. Patel College of Osteopathic Medicine, Nova Southeastern University, 3301 College Avenue, Fort Lauderdale, Florida 33314-7796*

[g] *Sylvester Comprehensive Cancer Center, University of Miami Miller School of Medicine, 1475 NW 12th Ave, Miami, FL 33136, USA*

* Corresponding authors

Dr. Leblanc:

*Phone:* +1 (305) 284-2194

*Locater code:* 0431

*Address:* University of Miami, Dept. Chemistry, 1301 Memorial Drive, Coral Gables, FL 33146, USA

Coral Gables, Florida 33146

*Email Address:* rml@miami.edu

Dr. Graham:

*Phone:* +1 (305) 321-4972

*Address: Department of Neurosurgery, University of Miami Miller School of Medicine, 1095 NW 14th Terrace, Miami, FL 33136, USA*

*Email Address:* rgraham@med.miami.edu

## Abstract

Carbon Dots (CDs) have recently attracted considerable amount of attention thanks to their well-documented biocompatibility, tunable photoluminescence, and excellent water solubility. However, CDs need further analysis before their potential use in clinical trials. Previously, we reported a new type of carbon nitride dots (CNDs) that displayed selective cancer uptake traits attributed to structural resemblances between CNDs and glutamine. Here, the effects of surface structural differences on the cellular uptake of CNDs are further investigated to understand their selective cancer cell uptake trend. Beyond enhanced drug loading on modified CNDs, our cytotoxicity, Western blot and bioimaging studies proposed that modified CNDs' cellular uptake mechanism is thoroughly linked with ASCT2 and LAT1 transporters. Therefore, CNDs have a promising trait in selective cancer cell targeting by utilizing highly expressed transporters on cancer cells. Additionally, drug loaded CNDs exhibited improved anti-cancer efficacies towards cancer cells along with good non-tumor biocompatibilities.

## 1. Introduction

Carbon dots (CDs), the latest member of the fluorescent nanomaterials family, have drawn a considerable attraction in the fields of cancer therapy, bioimaging, chemical sensing, and photocatalysis.[1,2] Some outstanding reasons laid behind the recent interest drawn by CDs for instance their well-documented biocompatibility, tunable photoluminescence, excellent water solubility, ease of production, and resistance to photobleaching in comparison to traditional

nanomaterials.[3] Generally, the term CDs have been used to label colloidal nanoparticles that are less than 10 nm in diameter, a great variety of chemical functional groups at their surface, and have a $sp^2/sp^3$ hybridized carbon core.

In literature, only a small number of existing nanomaterials have been used for clinical trials, and even fewer nanomaterials are approved for limited applications including cancer imaging and iron replacement.[4] Cytotoxicity still remains one of the major challenges for a greater clinical translation for metal based nanoparticles and quantum dots.[5] While traditional nanomaterials possess toxic traits, CDs present as a potentially safe nanocarriers since they are both highly biocompatible and water soluble. Since CDs are recent member of nanomaterial family, they need to be further analyzed and deeply investigated before they can be used in clinical trials.

With swift advances in both the fields of genomics and translational research, mankind pioneered an opportunity to understand the chemical and biological fundamentals of cancer by translating these laboratory discoveries into a personalized medicine.[6] Kathleen Sebelius, the former secretary of Health and Human Services, mentioned their goals related to personalized medicine are: " when doctors can truly prescribe the right treatment, to the right person, at the

right time, we will have a new level of precision and effectiveness that will provide the knowledge-driven power that is necessary to achieve our highest goals in healthcare reform — including more effective disease prevention and early disease detection." [7] Despite many examples of tailoring treatments using genetics for patients of various cancers, the successful implementation of a personalized medicine must assess factors beyond genetic information. It is required to incorporate new yet fundamental chemical and biological findings to advance these discoveries towards to clinical applications.[8,9]

Our group previously reported about the synthesis of carbon nitride dots (CNDs) as a targeted cancer therapy and selective bioimaging nanomaterial.[10] Urea and citric acid were chosen as precursor for the synthesis of CNDs. *In vitro* bioimaging studies using pediatric glioma cells (SJ-GBM2) were performed to analyze possible selective biolabeling and biodistribution within the cell membrane. Overall, CNDs selectively entered SJ-GBM2 tumor cells more efficiently while the cellular uptake was noticeably lower for normal human embryonic kidney cells (HEK293). We hypothesized that this observation was related to high surface structural resemblance of CNDs to the amino acid glutamine. To sustain rapid cell proliferation, cancer cells undergo metabolic reprogramming leading to an increased need for

amino acids compared to non-cancer cells. Glutamine is especially important for biosynthesis, energy production and redox homeostasis and as such cancers can become "addicted" to glutamine.[11] This dependence on glutamine may be considered cancers' Achilles heel therefore developing a CND nanocarrier targeting the glutamine transporters should increase the specificity toward cancer cells and thus, the efficiency of drug delivery.

To test and develop the previous hypothesis further, we modified the surface functional groups of CNDs to analyze their properties regarding selective cellular uptake of cancer cells. We, consequently, were able to manipulate the amount of surface primary amine and carboxylic groups. By changing the precursors' ratios in the beginning of the synthesis, we have synthesized CNDs with different ratios of surface functional groups. After meticulous characterizations of these modified CNDs, we conjugated doxorubicin (a very well-known cancer drug) on to the modified surface of CNDs. The doxorubicin conjugated CNDs were, subsequently, treated with different pediatric high-grade gliomas including glioblastoma (GBM) and Diffuse Intrinsic Pontine Glioma (DIPG), and high-risk neuroblastoma cell lines. According to our cell viability studies, the surface modified CNDs were able to carry more doxorubicin with exceptional cancer toxicity in addition with preserving their biocompatible

traits towards non-tumor cells. Moreover, to further analyze the cancer cell uptake of the

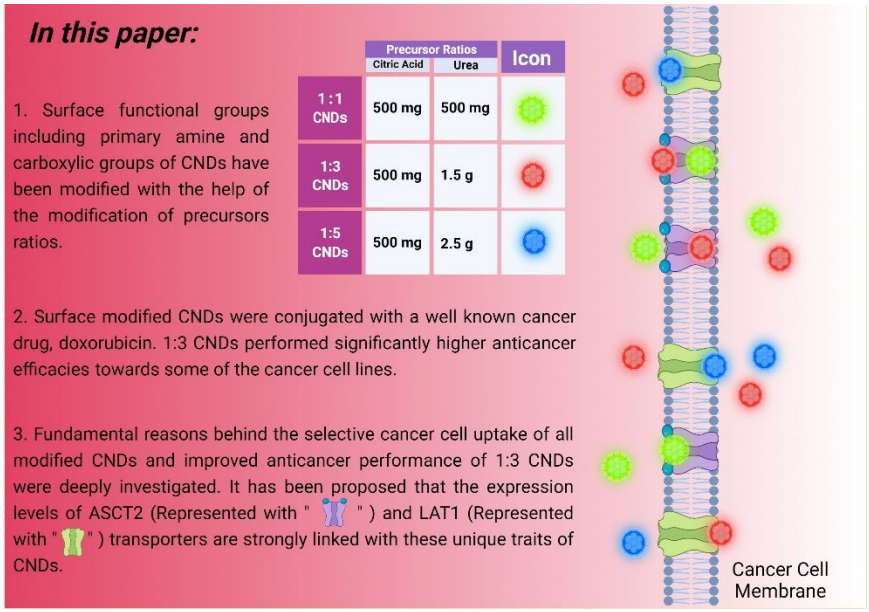


**Fig. 1** Highlights of this manuscript.

surface modified CNDs, we employed bioimaging studies with 5 different inhibitors. Our bioimaging results suggested that the cellular uptake mechanism of modified CNDs is highly related to the expression levels of amino acid transporters, specifically ASCT2 and LAT1. ASCT2 is the preferred amino acid transporter for glutamine while LAT1 preferentially transports large branched and aromatic neutral amino acids, such as tryptophan **(Fig. 1)**. Both ASCT2 and LAT1 are overexpressed in a wide range of tumors.[12] Although more analysis and investigation of their characteristics is still needed, CNDs appear extremely promising as versatile nanocarriers for future clinical trials of cancer.

## 2. Experimental Section

### 2.1. Materials Used

Anhydrous citric acid (purity > 99.5%), Urea, Doxorubicin hydrochloride ≥95% (by HPLC) , N-hydroxy succinimide (NHS), 1-ethyl-3-(3-dimethyl aminopropyl) carbodiimide hydrochloride (EDC), dithiothreitol (DTT), and lactic acid were purchased from VWR (West Chester, PA), Eastman Kodak Company (NY, U.S.A.), Sigma Aldrich (St Louis, MO), respectively. Deionized (DI) water was used for preparing all of the solutions and dialysis of carbon dots. MilliQ3 water purification system obtained from Millipore Sigma (Burlington, MA) was employed to purify the water. The surface tension of the purified deionized water is calculated as 72.6 $mN \cdot m^{-1}$ with a resistivity of 18 MΩ·cm, and a pH of 6.6 ± 0.3 at 20.0 ± 0.5 ˚C. Spectra pore dialysis tubing with a molecular weight cutoff (MWCO) of 100–500 Da was purchased from VWR (West Chester, PA) and was used for dialysis. The pediatric glioblastoma cell line SJ-GBM2 and the MYCN amplified neuroblastoma cell line SMS-KCNR was obtained from the Children's Oncology Group (COG, Texas Tech University, Health Science Center, TX, USA). Pediatric glioblastoma cell lines SF188 and KNS42 were generously provided by Dr. Chris Jones (Paediatric Oncology, The Institute of Cancer

Research, Sutton, United Kingdom). SJ-GBM2, SMS-KCNR, SF188 and KNS42 were maintained in RPMI media supplemented with 10% FBS and 1% penn/strep (Gibco, Carlsbad, CA). Diffuse Pontine glioma (DIPG) cell line NP53 was kindly provided by Dr. Oren Becher (Northwestern University Feinberg School of Medicine, Ann and Robert H. Lurie Children's Hospital of Chicago Illinois, USA). This cell line was derived from a mouse DIPG model induced by PDGF-B signaling, TP53 loss, and ectopic H3.3K27 expression.[13] DIPG cells were cultured in Complete NeuroCult™ Proliferation Medium (Stemcell Technologies, Vancouver, Canada) supplemented with 1% penn/strep. Mesenchymal stem cells (MSCs) originally derived from human bone marrow aspirates were obtained from Thermo Fisher Scientific and maintained in MEM alpha supplemented with 20% FBS and 1% penn/strep. Prior to drug treatment, MSCs were moved to media with 10% FBS. All cells were maintained at 37 ˚C in a humidified 5% CO2 incubator and routinely tested for mycoplasma using LookOut mycoplasma PCR detection kit (Sigma Aldrich, St Louis, MO). To guard against excessive cell passaging, newly received cell lines are routinely expanded with several cryovials frozen down for future use. The cell lines utilized in this study are not listed on the most recent NCBI database for misidentification and contamination of human cell lines.

## 2.2. Synthesis of 1:1, 1:3 and 1:5 CNDs

Carbon-nitride dots with different ratios of citric acid and urea were synthesized by following Liyanage et. al. via hydrothermal microwave-mediated procedure. [10] Briefly, 0.5 g of citric acid and 0.5, 1.5 and 2.5 g of urea were dissolved in 25 mL of DI water for the preparation of the 1:1, 1:3 and the 1:5 CND ratios, respectively. This mixture was left for stirring vigorously for overnight. Then the mixture was heated for 7 min (700 W) until all the water evaporated and mixture turned into black solid product. 15 mL of DI water was added on top to disperse the product and sonicated for 30 min. Then the dispersed CDs solution was centrifuged for 15 min at 1500 rpm twice to get rid of any precipitation. The supernatant was further purified via syringe filtrates with a filter membrane of 0.2 μm. The filtrate was dialyzed against DI water for 3 days by using 100-500 Da MW cutoff dialysis tubing. As final step, remaining water after dialysis was evaporated via rotavapor with heating to 70-80 $^{o}$C.

## 2.3. Characterization of the CND Ratios

The prepared CNDs were characterized by using UV-vis absorption in a 1 cm quartz cuvette (Starna Cells) using a Cary 100 UV−vis spectrophotometer (Agilent Technologies) in aqueous medium. A Horiba Jobin Yvon Fluorolog-3 with a slit width of 5 nm was performed

for measuring the photoluminescence emission spectra of the CND ratios along with using 1 cm path length quart cuvette. The Fourier Transform Infrared (FTIR) spectra were executed using a PerkinElmer Frontier with a universal ATR sampling accessary utilizing air as background. The mass spectroscopy was perpetrated with a Matrix-Assisted Laser Desorption/Ionization-Time of Flight (MALDI-TOF) mass spectrometry (MS) using a Bruker auto flex speed spectrometer. The AFM studies were conducted using an Agilent5420 atomic force microscope in the tapping mode. TEM studies were performed with a JOEL 1200× TEM. For the zeta potential measurement, a DLS nano series Malvern Zetasizer (Westborough, MA) was employed. XPS spectra were recorded by using a PHI 50 0 0 Versaprobe (Physical Electronics, Chanhassen, MN, USA) scanning X-ray photo electron spectrometer (monochromatic Al K-alpha X-ray source with 1486.6 eV energy, 15 kV voltage, and 1 mA anode current). For the quantification of doxorubicin loading, the circular dichroism (CD) analyses were performed by using a JASCO J-810 spectropolarimeter within the range of 275 to 550 nm using a 1 cm quartz cells (Starna Cells, Inc.; Atascadero, CA). Three batches of CNDs were analyzed by repeating each characterization methods.

## 2.4. Surface functional groups quantification

We implemented a fluorescence analysis using fluorescamine assay to calculate the number of primary amine groups on the surface of modified CNDs. A published process has been followed to perform this work.[14] Briefly, 2 mg of modified CND ratios was dispersed in 2 mL acetone/1×PBS (1:1) buffer solution. The prepared solutions of CND ratios were diluted by 100 times to prevent future errors caused from the emission saturation. Upon addition of 1,2-ethylenediamine (EDA) into fluorescamine, we analyzed the linear relationship between the molarity of primary amine groups and the fluorescence intensity of the solutions. The acquired fluorescence intensity from the addition of fluorescamine into modified CNDs aqueous dispersion was incorporated into the linear equation relationship. From this equation, quantification of primary amine groups on 2 mg of modified CNDs were calculated.

We employed a classical acid-base titration to quantify the number of carboxylic groups on the surface of modified CNDs. 0.5 mg $mL^{-1}$ stock solution of modified CNDs was prepared. Then, this stock solution was diluted into 0.02 mg $mL^{-1}$ concentration. The titration of this solutions was performed with the slow addition of 50 mL 0.005 mol $L^{-1}$ NaOH solution along with inserting the probe of SCHOTT Lab 850 benchtop pH meter. The titration was conducted until the pH meter shows pH around 7 for over 3 min waiting time. Finally, the volume of

added NaOH solution was recorded for the calculation of the carboxylic groups on modified CNDs.

## 2.5. Fluorescence quantum yield calculations

We calculated the fluorescence quantum yield (Φ) of CNDs by comparing the integrated area under the fluorescence curve and the absorbance intensity values using quinine sulfate and harmane as the reference standards. In literature, quinine sulfate and harmane have 54% and 83% quantum yield (QY), respectively when they are dissolved in 0.1 M $H_2SO_4$ (refractive index, $n_R$= 1.33, at 350 nm).[15] We dispersed modified CND ratios in DI water (refractive index, $n_R$= 1.33). Then, prepared solutions of CNDs were analyzed with UV-vis absorbance in the 1 cm path length quartz cuvette. The absorbance intensity was maintained under 0.05 a.u. and absorbance data was collected at 350 nm. Subsequently, the fluorescence emission spectra of some solutions of modified CNDs were obtained with the 350 nm excitation wavelength. The average of 5 repeats of absorbance intensities and integrated areas for the fluorescence emission spectra were fitted in the following equation,

Eq. (1): $$\Phi = \Phi_R \times (I / I_R) \times (A_R / A) \times (n^2 / n_R^2)$$

In this equation, $\Phi_R$, I, A, n symbols correspond to the literature QY of the standard, the integrated area under the PL curve, absorbance intensity at 350 nm, and the refractive index, respectively. Sub-script R is denoted for the reference.

## 2.6. Conjugation of doxorubicin on CNDs

6 mg of 1:1, 1:3, and 1:5 CNDs were dissolved in 2 mL of PBS (7.4 pH) solution. Then, 12.9 mg of 1-(3-dimethylaminopropyl)-3-ethylcarbodiimide hydrochloride (EDC) was dissolved in 1 mL of DI water and was added into the CNDs solution. The mixture was stirred at room temperature for 30 min. Then, 9.8 mg of N-hydroxysuccinimide (NHS) dissolved in 1 mL of DI water was mixed into the solution. After 30 min of stirring, 4.6 mg of doxorubicin dissolved in 1 mL of dimethyl sulfoxide (DMSO) was added to the solution. The entire mixture was stirred at room temperature overnight. Then the mixture was dialyzed by using 100-500 Da MWCO dialysis bag for 3 days. The DI water was replaced every 4–10 h. Finally, the frozen samples were lyophilized for 3 days to obtain the powdered product.

## 2.7. Cell viability studies

At 24 h prior to treatment, cells were seeded at a density of either $0.5 \times 10^5$ cells/ml (MSC), $1 \times 10^5$ cells/ml (SJ-GBM2, SMS-KCNR, KNS42) or $1.5 \times 10^5$ cells/ml (SF188 and NP53) in 100 µL in 96-well plates. Next, the cells were treated with 100 µL of different concentrations (0, 40, 80, 200, 400 nM) of the 1:1, 1:3, and the 1:5 CNDs. Cells also treated with 100 µL of different concentrations (10, 50, 100, 250 nm) of doxorubicin. Treatment was assessed after either 72 h or exposure or 3 h of exposure in which the CNDs and doxorubicin were removed and replaced with fresh media. Cell viability was determined by using the CellTiter 96 Aqueous One Solution Cell Proliferation Assay (MTS) (Promega Madison, WI). The absorbance was measured at 490 nm using BioTek Synergy HT plate reader. The average of 3 separate experiments were performed to present the data in which the viability was calculated as the relative percentage of non-treated cells. Finally, the standard error of the mean (SEM) was also computed for viability results.

## 2.8. Western blotting

For the Western blotting studies, we followed our previous protocol that has been published.[16] MSC, SJ-GBM2, SF188, SMS-KCNR, KNS42, NP53 cells were lysed in RIPA buffer and protein concentrations calculated by using BCA protein assay (BioRad Hercules,

CA). Equal amounts of protein (20 μg) was loaded onto 12 polyacrylamide gel (BioRad Hercules, CA) for electrophoresis and subsequently transferred onto nitrocellulose membranes. Then, these membranes were blocked for 1 h in 5% non-fat milk (Biorad, Hercules, CA) at room temperature (RT) and incubated with the primary antibody diluted in 2.5% BSA overnight at 4 degrees. ASCT2 transporter polyclonal antibody (SLC1A5) and LAT1 transporter polyclonal antibody (SLC7A5) were obtained from MyBioSource (San Diego, CA), Invitrogen (Waltham, MA). Finally, all membranes were incubated at room temperature with anti-mouse or anti-rabbit secondary antibodies for 1 h. Blots were processed by using SuperSignal™ West Pico Chemiluminescent Substrate (Thermo Scientific Waltham, MA).

### 2.9. *In vitro* bioimaging

MSCs and SJ-GBM2 cells were plated in 4-well plates (NUNC, Denmark) for imaging and incubated for 24 h for sufficient cell growth. Then, the media was removed; the cells were treated with 500 μL serum free DMEM and RPMI solutions containing 1 mg mL-1 of the 1:1, 1:3, and the 1:5 CNDs and further incubated for 1 hour. After this treatment, cells were washed with PBS and treated with 1 μg/mL Hoechst for 15 min. Then, cells were washed with PBS

two more times and fixed with 4% formaldehyde for 20 min. After fixation, 100 μL of citifluor antifade agent was added to the cells for 2 days. Finally, the cells were washed with PBS three times to wash off the antifade agent. The cells were subjected to fluorescence microscopy imaging by using a Floid Cell Fluorescent Microscope (Thermo Fisher Scientific, Waltham, MA). The same imaging settings were used for each group.

Additional bioimaging studies were performed with the presence of 5 different ASCT2 and LAT1 transporter competitive ligands. The ASCT2 transporter inhibitors, O-benzyl-D-serine (Benser), glutamine, (2S)-2amino-4-[bis[[2-[(3-methylphenyl)methoxy]phenyl]methyl]amino]-butanoic acid (V-9302) were purchased from Chemcruz (Dallas, TX), Gemini Biosciences (West Sacramento, CA), and Cayman Chemical (Ann Arbor, MI), respectively. The LAT1 transporter inhibitors 2-amino-bicyclo [2.2.1]heptane-2-carboxylic acid (BCH) and tryptophan were obtained from Gemini Biosciences (West Sacramento, CA), and Cayman Chemical (Ann Arbor, MI). The glioblastoma S-JGBM2 ($1 \times 10^5$) cells were divided into 4-well plates (NUNC, Denmark) for inhibitor imaging studies in 750 μL media and incubated for 24 h for sufficient cell growth. Next day, the cell media was aspirated, and the cells pretreated with inhibitors; Benser (60

mM), glutamine (60 mM), V-9302 (15 μM), BCH (15 mM), and tryptophan (60 mM) for 15 min. After this treatment, 500 μL DMEM and RPMI solutions containing 1 mg mL-1 of the 1:1, 1:3, and the 1:5 CNDs were added to cells and incubated for 1 hour. Then, cells were washed with PBS 2 more times and fixed with 4% formaldehyde for 20 min. After fixation, 100 μL of citifluor antifade agent was added the cells for 2 days. Finally, cells were washed with PBS 3 more times to wash off the antifading agent. The cells were imaged under fluorescence microscopy imaging by using a Floid Cell Fluorescent Microscope (Thermo Fisher Scientific, Waltham, MA). The same imaging settings were used for each group.

### 2.10. Image Analysis

The image analyses of modified CNDs were performed using ImageJ v.1.53i. PL intensity quantification analyses of images were performed using Graphpad Prism 9.3.1 software. The pixel counts per fluorescence intensity (grey scale) quantification of fluorescence intensities of cells were determined using ImageJ v.1.53i. The relative pixel count is the number of pixels with a given fluorescence intensity within a selected region of interest (either MSC or SJ-GBM2 cells), subtracted by the background pixels in that region. PL intensities are represented as a box plot. In boxplots, center bars represent medians and expand to the first and third

quartiles; whiskers extend to min/max data points. Statistically significant differences of PL intensities of images were determined using one-way analysis of variance (ANOVA) ($P \leq 0.001$) followed by Tukey's honest significant difference post hoc test ($P \leq 0.05$).

### 2.11. Statistical analysis

Significance of cytotoxicity and cell viability studies were calculated by performing Student's t-tests for all pairwise comparisons of the different treatments that were tested. All the results are presented as the mean±standard error of the mean (SEM). Significance was set at $p \leq 0.05$.

## 3. Results

### 3.1. Characterization of 1:1, 1:3, 1:5 CNDs

Our main goal was to modify the surface of CNDs for a larger investigation of their

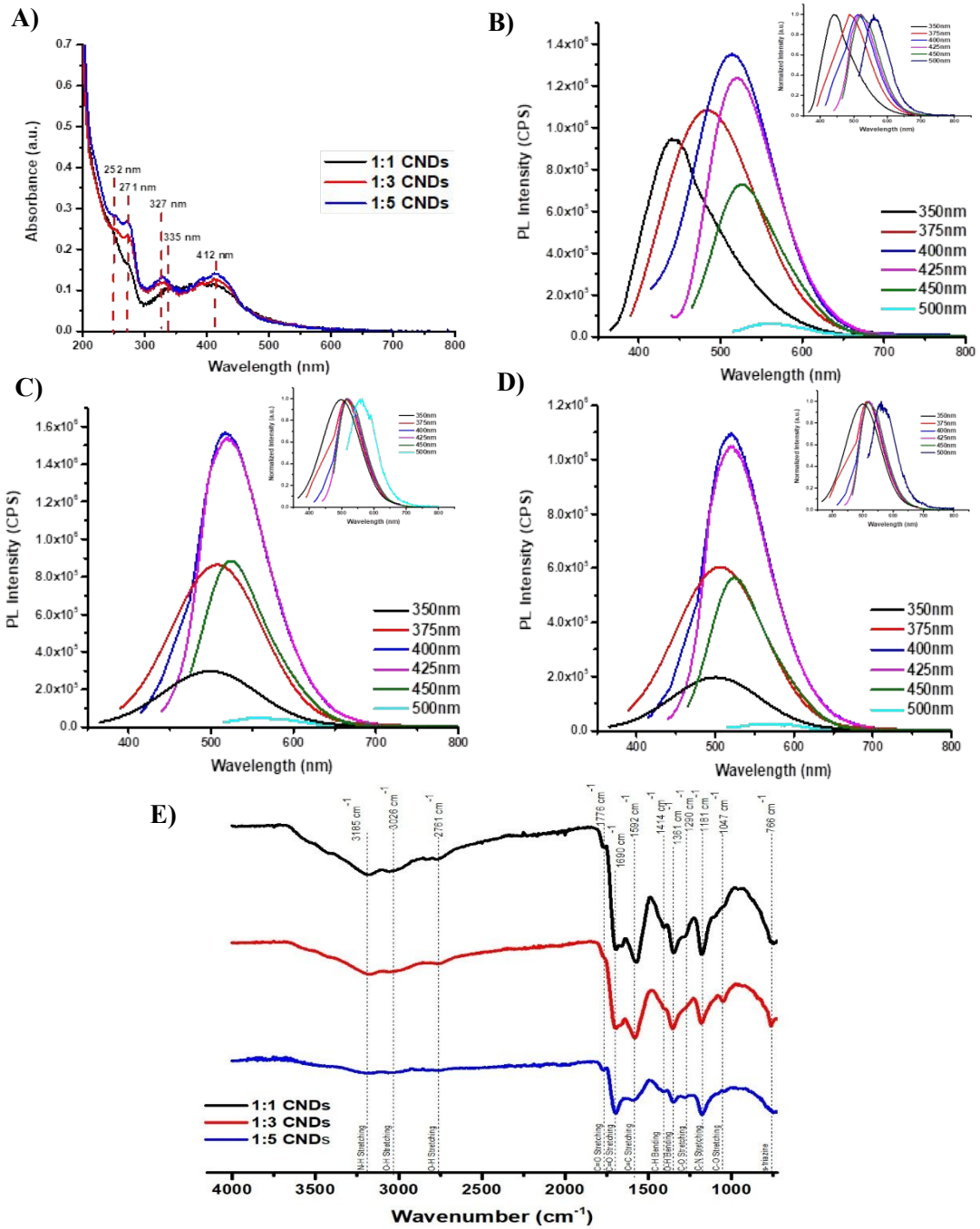


**Fig. 2 A)** UV–vis absorption spectra of modified CNDs (concentration = 0.1 mg/ml). **B, C, D)** PL emission spectrum of 1:1, 1:3,1:5 CNDs (concentration = $1 \times 10^{-6}$ mg/ml), respectively. Insets, normalized PL emission spectra of 1:1, 1:3, 1:5 CNDs. **E)** FTIR spectra of modified CNDs.

chemical and biochemical characteristics. It is for this reason that we have used different

proportions of precursors to synthesize CNDs. The modified CNDs were first characterized with UV-vis absorption spectra. Modified CNDs exhibited characteristic bands in the range of 200-400 nm **(Fig. 2, A)**. Previously, these bands were assigned to n− π* electronic transition of C=O groups and π−π* electronic transition of carbon nitride s-triazine rings.[10] On the other hand, both the 1:3 and the 1:5 CNDs presented a more prominent band at 412 nm, which was assigned to n− π* electronic transition of C-N and C=N groups.[17] Furthermore, the 1:3 and the 1: 5 CNDs spectra show the same absorption bands for π− π* electronic transition of C=C groups and n− π* electronic transition of C=O groups at 252, 271, 327, 335 nm wavelengths. When we analyzed the PL emission spectra of 1:3 and 1:5 CNDs, we noticed some differences compared to the 1:1 CNDs. For instance, there was a red shift for the emission bands excited with 350 and 375 nm. **Fig. 2, B** shows PL emission spectrum of 1:1 CNDs and maximum peaks for emission bands excited with 350 and 375 nm are at 442 and 483 nm respectively. Differing from the emission bands of the 1:1 CNDs, the 1:3 PL peaks are observed at 498 and 507 nm for the same excitation wavelengths **(Fig. 2, C)**; the 1:5 produces PL maximum peaks at 501 and 507 nm for the same excitation wavelengths **(Fig. 2, D)**. All three types of CNDs have excitation dependent emission properties which are observed from the normalized PL spectra.

Currently, there is no agreement about the mechanism behind the excitation dependent PL behavior of CDs. Moreover, the most prevalent theories behind this behavior were attributed to the presence of surface electronic states, incorporation of fluorophores into the particles structure, and dot-to-dot variations which ultimately led to the excitation-dependent ensemble properties.[18] We observed distinct differences between the FTIR bands between the 1:1, the 1:3 and the 1:5 CNDs **(Fig. 2, E)**. Firstly, both the 1:3 and the 1:5 CNDs had significant decreases in the prominence of the 3026 $cm^{-1}$ band which was assigned to $\nu_{O-H}$ from the -COOH groups. This result presented the first confirmation that there is a decrease in in the amount of -COOH groups in the modified 1:3 and the 1:5 CNDs. Conversely, another imperative finding was observed at the 1690 $cm^{-1}$ band. This band was assigned to $\nu_{C=O}$ of amide functional groups. Both the 1:3 and the 1:5 CNDs showed more prominent amide bands than the 1:1 CNDs. In other words, there was an increase in the amount of $-NH_2$ groups on both the 1:3 and the 1:5 CNDs. The remaining FTIR bands peaked at 3185, 2761, 1776, 1592, 1414, 1361, 1290, 1181, 1047, and 766 $cm^{-1}$ were assigned to $\nu_{N-H}$, $\nu_{O-H}$, $\nu_{C=O}$, $\nu_{C=C}$, $\delta_{C-H}$, $\delta_{O-H}$, $\nu_{C-O}$, $\nu_{C-N}$, $\nu_{C-O}$ and s-triazine, respectively. [15,19,20]

We have investigated morphological and size distribution properties of modified CNDs by AFM and TEM studies. In our previous study, we mentioned that 1:1 CNDs retain a height profile between 1.0-3.8 nm and a diameter ranging between 2.0-3.5 nm.[10] The 1:3 CNDs' height is in the range of 1.6-2.0 nm **(Fig. S1, A)** while their average diameter is between 2.7-3.1 nm **(Fig. S1, B)**. For the 1:5 CNDs, they had a height profile between 1.3-2.1 nm and average diameter between 2.7-3.2 nm **(Fig. S1, C, D)**. Both the 1:3 and the 1:5 CNDs present similar height profiles to their average diameters, verifying a spherical shape in general. In summary we did not notice a relevant change in the morphology and size of CNDs when the ratio of urea to citric acid varied.

To further characterize the modified CNDs, we calculated quantum yield (QY), quantified the amount of surface -COOH and -NH2 groups, found the surface charge, and obtained the MALDI-TOF main +1 Ionization peak for the 1:1, 1:3 and the 1:5 CNDs **(Fig. 3, A)**. Accordingly, we have measured the QY of the three types of modified CNDs, but we did not observe a drastic change in their brightness. The original CNDs (1:1) had QY around 11.53 % while modified 1:3 and 1:5 CNDs showed QY values of 12.54 % and 9.53 % respectively. To assess the variations in the amount of surface -COOH and -$NH_2$, we employed a

straightforward acid-base titration and a fluorescamine assay. As a result, we obtained further

**A)**

| Sample | QY (%) ± STD | Number of -COOH groups on the surface (mmol/g) | Number of -$NH_2$ groups on the surface (mmol/g) | Zeta Potential (mV) | MALDI-TOF +1 Ionization Main Peak (m/z) |
|---|---|---|---|---|---|
| **1:1 CNDs** | 12 ± 2.0 | 0.30 | 0.007 | -38.8 | 750 |
| **1:3 CNDs** | 12 ± 2.1 | 0.20 | 0.010 | -23.4 | 750 |
| **1:5 CNDs** | 10 ± 1.8 | 0.18 | 0.024 | -20.4 | 750 |

**B)**

| Sample | Carbon Species (%) | | | | Oxygen Species (%) | | | Nitrogen Species (%) | | |
|---|---|---|---|---|---|---|---|---|---|---|
| | C $sp^2$ | C-X (X= N, O) | C=O | COOH | -OH | C=O | COOH | N Pyridinic | $NH_2$ | N□ |
| **1:1 CNDs** (C: 64%, O: 24%, N: 12%) | 54 | 17 | 24 | 5 | 4 | 78 | 18 | 17 | 50 | 33 |

**C)**

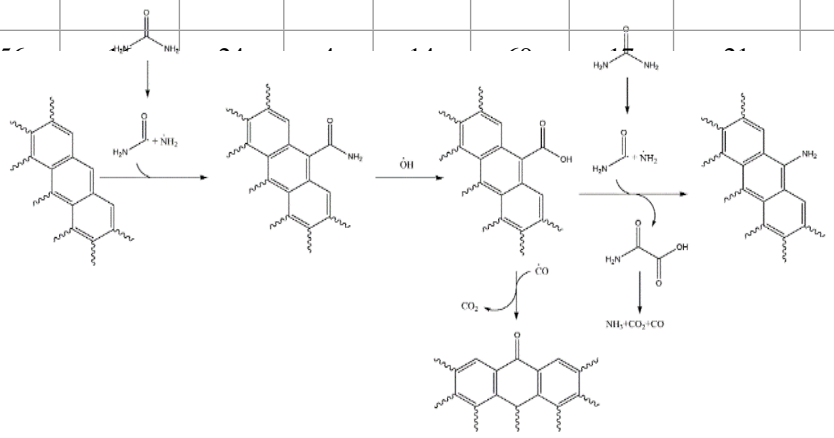

**Fig. 3** **A)** Table for Quantum yield, Number of -COOH and -NH2 Groups on the surface, Surface Charge and MALDI-TOF Main +1 Ionization peak of 1:1, 1:3 and 1:5 CNDs. **B)** Table for Output of XPS analysis for carbon, oxygen, and nitrogen. **C)** Schematic representation of Radical carboxylation of CND edges.

confirmation that the amount of surface -COOH groups is less in both the 1:3 and the 1:5 CNDs than the 1:1 CNDs **(Fig. 3, A)**. For each gram of 1:1, 1:3 and 1:5 CNDs, there were 0.3, 0.2, and 0.184 mmol of -COOH groups, respectively. Supportably, the fluorescamine assay confirmed the results of the FTIR by quantifying the surface -$NH_2$. Specifically, the number of

surface groups are 0.007 mol/g, 0.010 mol/g, 0.024 mol/g for the 1:1, 1:3, and the 1:5 CNDs' samples respectively. **(Fig. 3, A)**. Next, the zeta potential measurements revealed that the 1:1, 1:3 and the 1:5 CNDs form -38.8, -23.4, and -20.4 mV respectively **(Fig. 3, A)**. Furthermore, the formation mechanism of these CNDs should be based on two steps. The first step includes the condensation reaction between the amine groups of urea and the terminal carboxylic component of citric acid, eventually, resulting in the formation of a polyamide. These polyamide structures serve as formation seeds for the second step which involves carbonization via continuous heating. Thus, keeping the citric acid (carbon source) amount fixed should also assist in maintaining the formation of seeds constant. From this point in theory, modified CNDs should form a similar number of seeds and then follow similar carbonization routes that finally results in similar particle mass. MALDI-TOF main +1 ionization peaks of modified CNDs support this hypothesis by demonstrating main peaks close to 750 for all samples **(Fig. 3, A)**.

Next, XPS studies achieved to further analyze the surface functional groups of CNDs. **Fig. S2** displays XPS core levels for the C 1 s, N 1 s and O 1 s orbitals of the modified CNDs. C1s signal shows the presence of a relatively low amount of $sp^2$ hybridized carbon (284.7 eV) for each sample that slightly increased by the increment of citric acid/urea ratio with percentage

of up to 54-58 % with an increment of C $sp^2$ for ratio of 1:3 and 1:5 CNDs **(Fig. S2, A, a, b, c)**. An opposite trend was observed for carboxylic functionalities (289.7 eV C1s, 532.7 eV O1s) **(Fig. S2, A, d, e, f)**. Considering the O 1s signal, carboxylic decrement was also detectable from the 1:1 to the1:3 CNDs while carbonyl residues percentages did not show any appreciable trend. N 1s signal showed an increment of amine functions (400.1 eV) with the decrement of citric acid/ urea ratio. Furthermore, an increment of pyridinic (399.4 eV) and a decrement of NQ (nitrogen species included into the graphitic plane like the heptazine structures, 401.4 eV) were observed **(Fig. S2, A, g, h, i)**. These trends are summarized in **Fig. 3, B**. XPS analysis of modified CNDs is crucial to understand their biological intrinsic behaviors which will be further discussed at next sections.

The decrement of citric acid/urea ratio led to a radical rich environment that promoted aromatic condensation as proved by the increment of $sp^2$ CNDs' carbon. The heterolytic cleavage of C-N bond of urea did not induce the insertion of nitrogen into the aromatic plane or into the formation of biuret but as an amine group. The nitrogen rich CNDs displayed a decrement of carboxylic groups reasonably located on the edges accordingly to Lerf-Klinowski model. [21] The decreased number of carboxylic groups with the decrement of citric acid/urea

ratio could be explained by the radical mechanism reported in **Fig. 3, C**. The radical rich environment could lead to an improved reactivity of exposed edges with a partial replacement of carboxylic moieties with amine through the radical formation of a carbon dioxide, ammonia, and carbon monoxide. The massive presence of carbon monoxide supports the presence of a great amount of carbonyl residues produced though radical insertion or the carbonyl on the edges with or without carboxylic replacement. Considering all points raised above, the increase amount of urea induced an increment in shell functionalities with a decrement of nitrogen doped aromatic layer. Thus, both the 1:3 and the 1:5 CNDs are characterized with a more hydrophobic core and more polar external shell compared to the 1:1 CNDs.

### 3.2. Doxorubicin conjugation and quantification on modified CNDs

Here, we studied modified CNDs' nanocarrier properties by conjugating them with

doxorubicin, an anticancer drug. It has been known that doxorubicin has significant side effects

towards healthy cells.[22] The use of nanocarriers such as CDs should limit the side effects by

achieving a targeted delivery of doxorubicin to cancer cells. We loaded doxorubicin on the

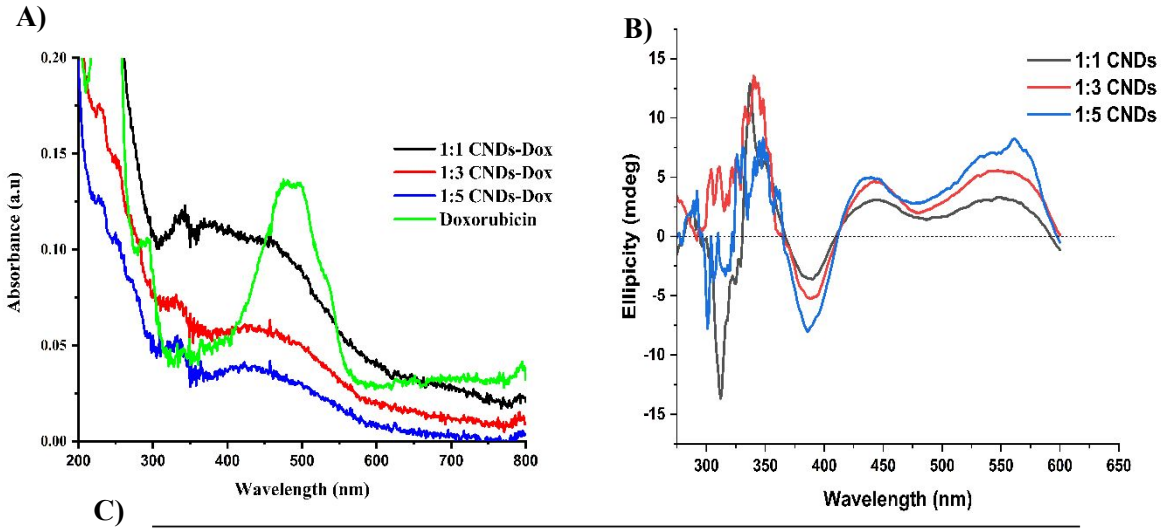


C)

| Sample | Amount of doxorubicin loaded per mg of conjugate (µmol/g) ± STD |
|---|---|
| 1:1 CNDs-Dox | 0.41 ± 0.03 |
| 1:3 CNDs-Dox | 0.51 ± 0.03 |
| 1:5 CNDs-Dox | 0.52 ± 0.03 |

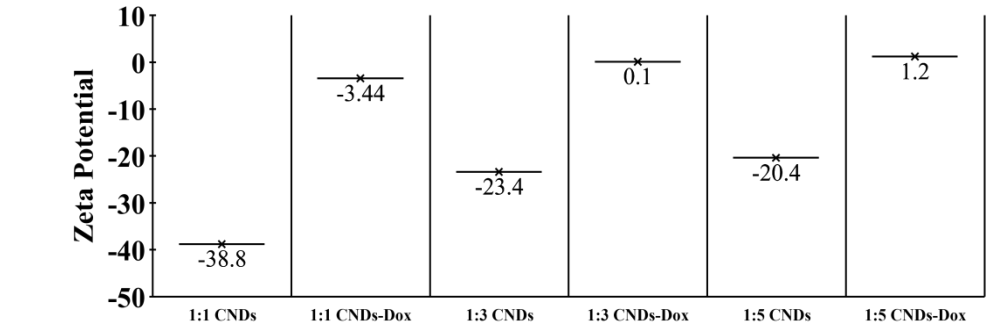


**Fig. 4 A)** UV-vis absorption spectra of Dox, 1:1 CNDs-Dox, 1:3 CNDs-Dox and 1:5 CNDs-Dox conjugates. **B)** Circular Dichroism (CD) spectra of 1:1 CNDs-Dox, 1:3 CNDs-Dox and 1:5 CNDs-Dox conjugates. **C)** Table for amount of doxorubicin loaded per mg of each conjugate. D) Table for comparing the differences between zeta potential (surface charge) measurements of surface modified CNDs before and after doxorubicin conjugation.

surface of modified CNDs by creating carbodiimide crosslink between the CNDs and the loading cargo. A long-established EDC/NHS bioconjugation between CNDs and doxorubicin

was performed. **Fig. 4, A** shows UV-vis absorption spectra of the purified 1:1, 1:3 and the 1:5 CNDs conjugated with doxorubicin. Doxorubicin has a specific absorption and at 490 nm. The same band at 490 nm appears in 1:1, 1:3, and 1:5 CNDs-Dox spectra, attesting to the achievement of a successful conjugation. We quantified the loaded doxorubicin on the modified CNDs using a technique previously established in our lab.[23] This analytical tool is based on the chirality of the molecules. The Circular Dichroism (CDH)'s working principle involves the differential absorption of left and right circularly polarized light. CNDs don't exhibit a CDH signal by themselves. However, when a chiral molecule is conjugated on the CNDs, it can be detected with CDH. Therefore, by using these features, we can create a calibration curve and calculate the amount of the doxorubicin loaded to the CNDs (**Fig. 4, B**). The drug loading amounts (**Fig. 4, C**) were found to be 0.41, 0.51, and 0.52 μmol/g for the 1:1, 1:3, and the 1:5 CNDs, respectively. This might appear a rather surprising result, considering the similar amount of available -COOH sites on the surfaces of modified CNDs. However, isoelectronic point (pI) of the molecule which donates -$NH_2$ groups is very important for the mechanism of EDC/NHS coupling.[24] Additionally, molecules with higher pI will be accepted as a base and their EDC/NHS conjugation will be decreased with highly negative structures

that donates -COOH groups.[24] Doxorubicin's pI is at 8.40.[25] Thus, doxorubicin is included in the category of basic structures. From this point, the 1:1 CNDs carry the highest negative surface charge comparing to the 1:3 and the 1:5 CNDs which may result in more repulsions of doxorubicin and lower coupling with its surface -COOH groups.

Finally, **Fig. 4, D** represents the difference between the surface charges of modified CNDs before and after doxorubicin conjugations. As a general outcome of the occupation of surface carboxylic groups with the conjugation of doxorubicin, all modified CNDs conjugated with this drug showed a significant decrease in the negative charge of the surface. Additionally, 1:3 and 1:5 CNDs were even slightly positive charged after the doxorubicin conjugations. Last but not least, **Fig. S3** exhibits AFM images of modified CNDs after the conjugation with the doxorubicin. In this figure, the height profile of the 1:1, 1:3 and 1:5 CNDs-Dox conjugates from AFM studies possess a range between 1.5-4.1 nm. Moreover, we have shown that 1:1, 1:3, 1:5 CNDs alone before any surface conjugations, have height profile ranges 1.0-3.8 nm, 1.6-2.0 nm, 1.3-2.1 nm, respectively. Comparing the AFM height profiles of modified CNDs before and after doxorubicin conjugations, it can be seen that there were slight increase in the overall size of the nano systems upon with doxorubicin conjugations.

### 3.3. *In vitro* cell viability studies

Here, we performed two separate *in vitro* studies with different time intervals towards a non-tumor cell line, namely MSC, and five different aggressive cancer cell lines, SJ-GBM2, KNS42, SMS-KCNR, NP53, and SF188. Nanocarriers are not able to stay around the tumor site for 72 hours in a more complex environment.[26] Therefore, in addition to 72 hours, we included a shorter treatment period of 3 hours to mimic more realistic scenario. Moreover, as discussed previously, original 1:1 CNDs have shown a selective cancer cell uptake towards a glioblastoma cell line, named SJ-GBM2.[10] To further study this selective cancer cell uptake towards SJ-GBM2, we applied more studies and collected data for our modified CNDs with this cell line. Additionally, we wanted to expand our studies to include additional pediatric high-grade glioma (KNS42, NP53, and SF188) and neuroblastoma (SMS-KCNR) cell lines to examine the cancer selective uptake of modified CNDs. Since myc oncoproteins are known to drive glutamine uptake and metabolism in cancer cells, we specifically included c-myc amplified SF188 and n-myc amplified KNS42 and SMS-KCNR cell lines.[27–30] Both the 1:3 and the 1:5 CNDs-DOX conjugates do not have significant change regarding the 3-hours cell viabilities towards non-tumor MSC cells when compared to the 1:1 CNDs **(Fig. 5, A)**.

Moreover, the 1:3 and the 1:5 CNDs-DOX conjugates performed notable anticancer efficacy

towards four glioblastoma cell lines: SF188, NP53, KNS42, and SJ-GBM2, and one

**A)**

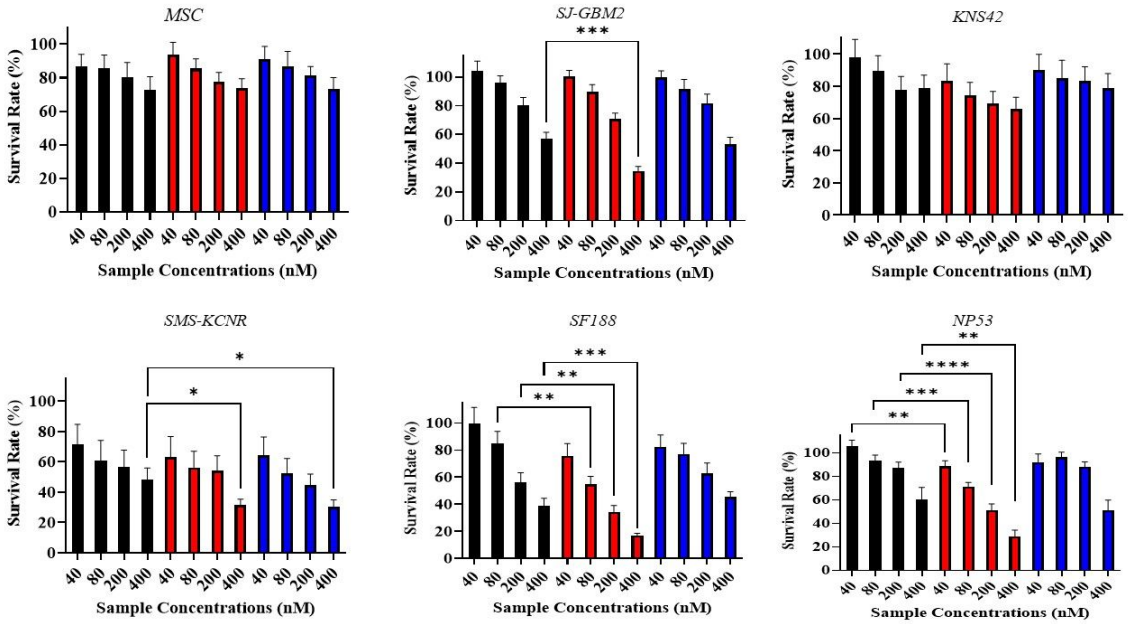


**B)**

| Cell Line | 1:1 CNDs-Dox Conjugates | | 1:3 CNDs-Dox Conjugates | | 1:5 CNDs-Dox Conjugates | | IC50 values of dox (nM) ± SEM |
|---|---|---|---|---|---|---|---|
| | IC50 values (nM) ± SEM | Amount of dox present at the IC50 points (nM) | IC50 values (nM) ± SEM | Amount of dox present at the IC50 points (nM) | IC50 values (nM) ± SEM | Amount of dox present at the IC50 points (nM) | |
| MSC | >400 | --- | >400 | --- | >400 | --- | >250 |
| SJGBM2 | >400 | --- | 298 ± 57 | 0.18 | >400 | --- | >250 |
| KNS42 | >400 | --- | >400 | --- | >400 | --- | >250 |
| SMSKCNR | 330 ± 55 | 0.16 | 241.2 ± 34 | 0.15 | 210 ± 45 | 0.14 | >250 |
| SF188 | 261.7± 30 | --- | 105.6± 27 | 0.18 | 361.4 ± 47 | --- | 209.8 ± 30 |
| NP53 | >400 | --- | 186.2 ± 16 | 0.068 | 349.9 ± 74 | 0.23 | >250 |

**Fig. 5 A)** 3-hours exposure cell viability results of 1:1 CNDs-Dox (Black), 1:3 CNDs-Dox (Red) and 1:5 CNDs-Dox (Blue) conjugates **B)** Table for IC50 values and amount of dox present at the IC50 points of CNDs-Dox conjugates, and IC50 values of doxorubicin alone. Results are expressed as % of survival rate. Values are means (nM) ± SEM (n = 12). P was accepted as 0.05.

neuroblastoma, SMS-K-CNR **(Fig. 5, A)**. The 1:3 CNDs, conversely, achieved the best

**A)**

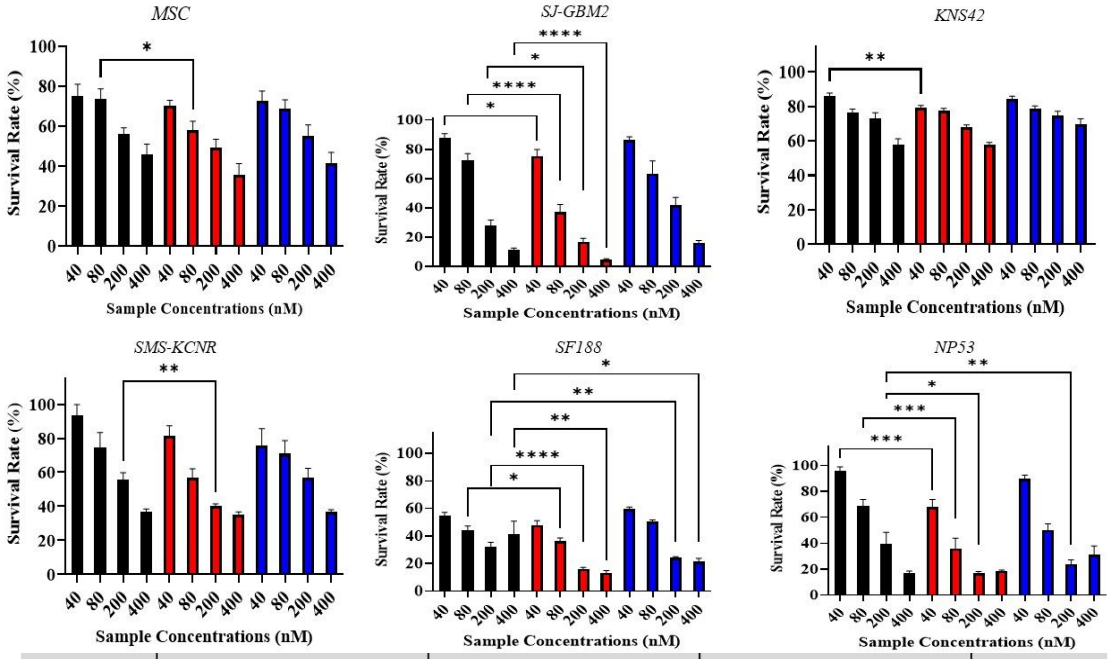


**B)**

| Cell Line | 1:1 CNDs-Dox Conjugates | | 1:3 CNDs-Dox Conjugates | | 1:5 CNDs-Dox Conjugates | | IC50 values of dox (nM) ± SEM |
|---|---|---|---|---|---|---|---|
| | IC50 values (nM) ± SEM | Amount of dox present at the IC50 points (nM) | IC50 values (nM) ± SEM | Amount of dox present at the IC50 points (nM) | IC50 values (nM) ± SEM | Amount of dox present at the IC50 points (nM) | |
| MSC | 323.7 ± 28 | 0.17 | 164 ± 57 | 0.10 | 257 ± 77 | 0.18 | 53.9 ± 13 |
| SJGBM2 | 125.2 ± 63 | 0.064 | 72.2 ± 23 | 0.046 | 134.3 ± 64 | 0.0.087 | 32.3 ± 8 |
| KNS42 | > 400 | --- | > 400 | --- | > 400 | --- | > 250 |
| SMSKCNR | 237.5 ± 60 | 0.12 | 148.4 ± 41 | 0.095 | 230.4 ± 102 | 0.15 | 77.3 ± 2 |
| SF188 | 46.1 ± 13 | 0.024 | 32.8 ± 9 | 0.021 | 68.7 ± 8 | 0.044 | 11.9 ± 4 |
| NP53 | 148.3 ± 58 | 0.076 | 62.2 ± 14 | 0.040 | 120.3 ± 21 | 0.078 | 22.1 ± 5 |

**Fig. 6 A)** 72-hours exposure cell viability results of 1:1 CNDs-Dox (Black), 1:3 CNDs-Dox (Red) and 1:5 CNDs-Dox (Blue) conjugates **B)** Table for IC50 values and amount of dox present at the IC50 points of CNDs-Dox conjugates, and IC50 values of doxorubicin alone. Results are expressed as % of survival rate. Values are means (nM) ± SEM (n = 12). P was accepted as 0.05.

anticancer efficacy among the three modified CNDs-Dox conjugates. The 1:3 CNDs' $IC_{50}$

values were as low as 105.6 nM **(Fig. 5, B)**. For most cases, 1:3 CNDs-Dox anticancer efficacies were better than the standalone doxorubicin's toxicity **(Fig. 5, B, C)**. We observed that all cell lines exhibited a traditional dose dependent inhibition log curves **(Fig. S4, A)**. Subsequently, the same cytotoxicity experiments were performed for 72-hour incubations (**Fig. 6, A).** Due to the initiation of passive diffusion after a significant period of time, CNDs start to get in with passive cell uptake pathways such as endocytosis. Therefore, we have observed higher toxicity for all modified CNDs-Dox conjugates and doxorubicin for the 72-hour treatments. Additionally, when we compare the viability results of the 1:1 CNDs with the 1:3 and the 1:5 CNDs, we did not observe a significant change in biocompability. From the same perspective, it was not suprising to see much higher anticancer efficacy of the the modified CNDs-Dox conjugates towards the cancer cell lines **(Fig. 6, A)**. Regarding the $IC_{50}$ values of the 72 hours treatments, the 1:3 CNDs-Dox conjugates generated results as low as 32.8 nM **(Fig. 6, B)**. Similarly, all cell lines demonstrated traditional dose dependent inhibition log curves **(Fig. S4, B)**. Finally, we calculated the amount of doxorubicin present on the IC50 concentrations of CNDs-Dox conjugates **(Fig. 6, C)**. With more precise cancer cell delivery of much less concentration of doxorubicin, we succeed to obtain not only improved anti-cancer efficacy but also reduced side effects to non-tumor cells. To sum up, the 1:3-CNDs-Dox conjugates performed the highest anticancer efficacies for most cases at the concentrations tested. 1:5 CNDs-Dox conjugates carry higher numbers of doxorubicin on their surface, but

the 1:3-CNDs-Dox conjugates were better at anti-cancer efficacy. Therefore, we hypothesize that because there is a difference in their cellular uptake mechanisms, the modified CNDs-Dox conjugates produced different anticancer efficacies. To support our hypothesis, we performed both Western blot and bioimaging studies.

### 3.4. Western blot analysis

We tested the transporter expression levels on the 6 cell lines for ASCT2 and LAT1 transporters. We chose ASCT2 and LAT1 transporters for Western blotting since the ASCT2 and the LAT1 transporters are the most common highly expressed transporters on large populations of cancer cells and CNDs surface functional groups resembles to ASCT2 and LAT1 amino acids.[31] Briefly, amino acid recognition mechanism of ASCT2 is based on the exchange of small amino acids via the variation in the concentration of $Na^+$ ion at the outer cell microenvironment.[32] On the other hand, LAT1 transporter's amino acid recognition is independent from both the $Na^+$ ion concentration and the pH of the outer cell microenvironment. LAT1 transporters form a heterodimeric complex with the glycoprotein 4F2hc to import amino acids.[33] **Fig. S5, A** presents our Western blot analysis for these two

transporters on the cell lines that have been employed for cytotoxicity. Firstly, all modified CNDs-Dox conjugates performed poor anticancer effects for KNS42 cell line **(Fig. 5, B and Fig. 6, B)**. If we correlate this data with our Western blot analysis, we can see that KNS42 cell line does not express high levels of the ASCT2 and the LAT1 transporters which may result in low cellular uptake for our CNDs-Dox conjugates **(Fig. S5, A)**. The SJ-GBM2, SF188 and SMS-KCNR cell lines on the other hand express high levels of ASCT2 transporters which can lead to higher cellular uptake and anticancer efficacy for the 1:3 CNDs-Dox conjugates. Moreover, if we look at the cases where LAT1 expression level is appreciable such as for the SMS-KCNR cell line, we observed that the anticancer efficacy of the 1:5-CNDs-Dox conjugates improves. Considering both the Western blot studies and the cytotoxicity results, we hypothesized that the 1:1 and 1:3-CNDs are more prone to be transported by both the ASCT2 and the LAT1 transporters while the 1:5-CNDs tend to enter cells through LAT1 transporters **(Fig. S5, B)**. The amino acid recognition mechanisms of these two transporters also support our hypothesis. For instance, the ASCT2 transporter recognizes amino acids that resembles glutamine, alanine, and threonine which possess functional groups including -COOH, $-NH_2$, and -OH on their structure. 1:1 and 1:3 CNDs have these functional groups,

especially -OH, on their surface. On the other hand, the LAT1 transporter recognizes amino acids by forming dimeric complex structures with membrane glycoproteins. Both all modified CNDs carry significant amounts of -COOH and -$NH_2$ groups to be recognized as one of the LAT1 transporter amino acids such as phenylalanine, tryptophan, and tyrosine. We further tested our claim about the cellular uptake mechanisms for both the 1:1, 1:3 and the 1:5 CNDs with *in vitro* bioimaging studies.

### 3.5. *In vitro* bioimaging

In this paper, in addition to performing imaging studies with modified CNDs, we have designed bioimaging studies to assess the uptake mechanisms of these CNDs. We first demonstrated bioimaging studies of the modified CNDs by using one non-tumor cell line, MSC, and one glioblastoma cancer cell line, SJ-GBM2. Control groups have shown that there was no PL leakage from blue to green channels or vice versa. Here, the green channel was attributed to image modified CNDs, and the blue channel was assigned to image Hoechst nucleus staining dye. The modified CNDs treatment did not affect the cell morphology and viability. As can be seen from **Fig. 7**, **A,** 1:3 and 1:5 CNDs were able to keep the same trait as 1:1 CNDs by selectively entering cancer cells at higher rates. The 1:3 CNDs illustrated the

significant increase in the green PL intensity for both the MSC and the SJ-BM2 cell lines

compared to the 1:1 CNDs **(Fig. 7, B, C, D)**. Meanwhile, the 1:5 CNDs also displayed

significant PL brightness to the 1:1 CNDs for both the non-tumor and the cancer cells

bioimaging **(Fig. 7, B, C, D)**. To further investigate cellular uptake properties of the modified

CNDs, we implemented bioimaging studies with the presence of the ASCT2 and the LAT1

transporters' competitive ligands **(Fig. 8, A)**. We selected five competitive inhibitor ligands to

work: benser, glutamine, V-9302, BCH, and tryptophan. It has been assessed in previous

studies that cellular uptake mechanisms of competitive inhibitors of benser, glutamine, and V-

9302 is directly related to the ASCT2 transporter levels.[34–36] Further studies have shown that

BCH and tryptophan are up taken by LAT1 transporter on the cells.[37,38] We hypothesized that

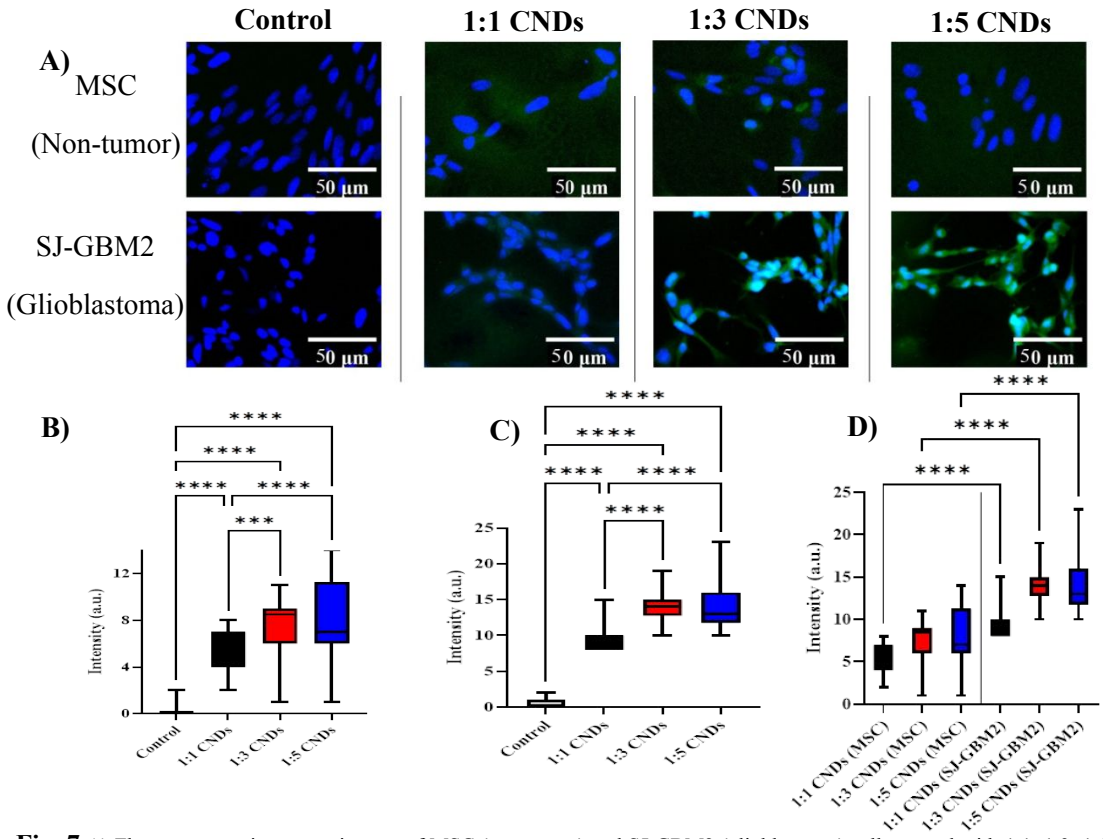


**Fig. 7 A)** Fluorescence microscopy images of MSC (non-tumor) and SJ-GBM2 (glioblastoma) cells treated with 1:1, 1:3, 1:5 CNDs. Both cell lines were treated with 1 mM concentration of modified CNDs for 1 h. Scale bars are 50 µm. Excitation wavelength: Blue, 358 nm, Green, 488 nm. **B)** Green PL intensity quantification for MSC (non-tumor) images of modified CNDs. Values are means ± range (n=30). **C)** Green PL intensity quantification for SJ-GBM2 (glioblastoma) images of modified CNDs. Values are means ± range (n=30). **D)** One-way (Anova) statistical comparison for MSC (non-tumor) and SJ-GBM2 (glioblastoma) green PL intensity of modified CNDs. Values are means ± range (n=30). *P < 0.05, **P < 0.01, ****P < 0.0001. In boxplots, center bars represent medians and expand to the first and third quartiles; whiskers extend to min/max data points.

if the possible cell uptake mechanism of the 1:1, 1:3 and the 1:5 CNDs are connected with the

ASCT2 and the LAT1 transporters, then their PL intensity for bioimaging should be affected

in the presence of the competitive molecules that occupies the same transporters for cell uptake.

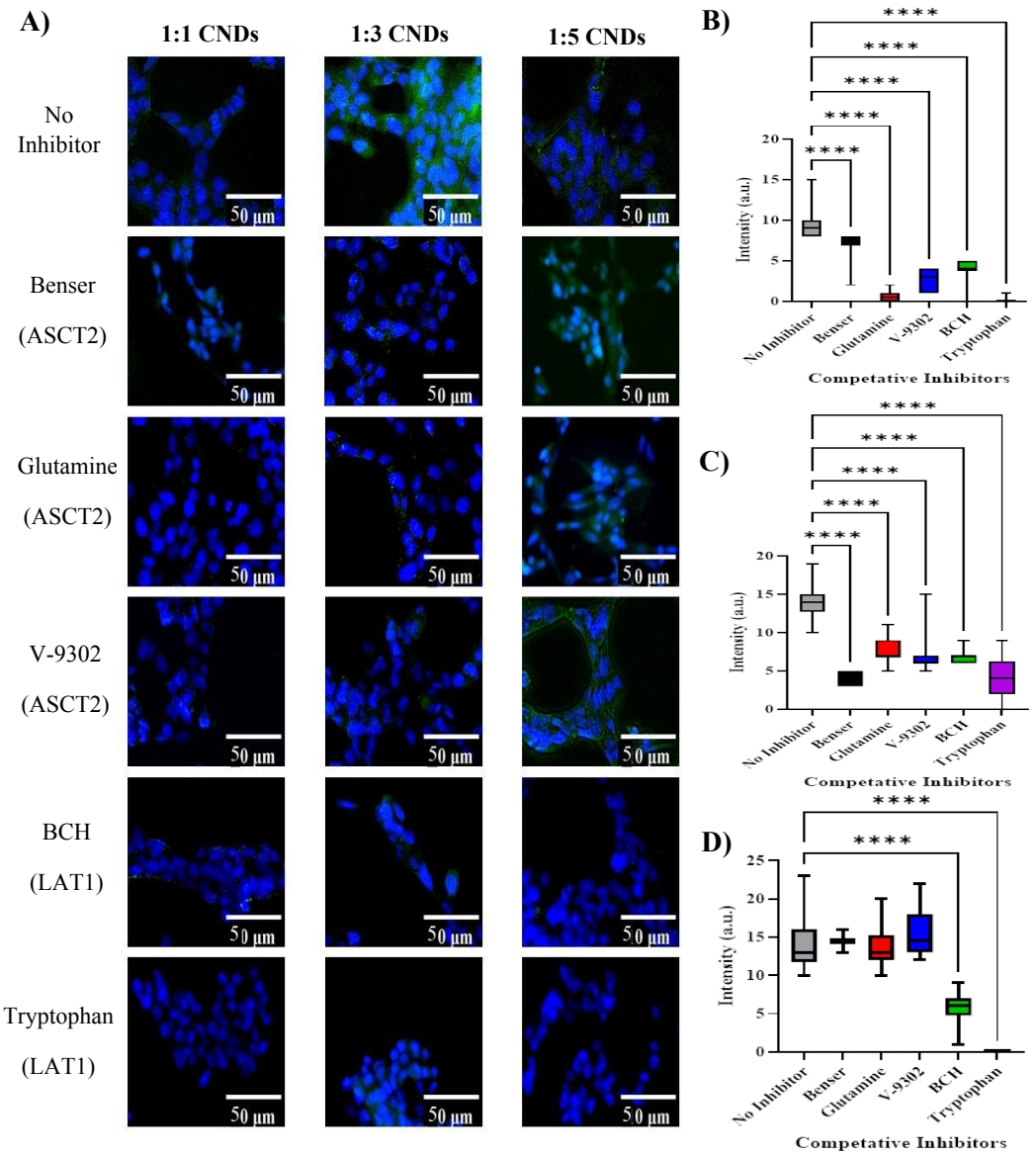


**Fig. 8** **A)** Fluorescence microscopy images of SJ-GBM2 (glioblastoma) cells treated for an hour with 1 mM of 1:1, 1:3 and 1:5 CNDs, 60mM of benser, 60mM of glutamine, 15µM of V-9302, 15mM of BCH, and 60mM of tryptophan. Scale bars are 50 µm. Excitation wavelength: Blue, 358 nm, Green, 488 nm. **B, C, D)** Green PL intensity One-way (Anova) quantification of 1:1, 1:3 and 1:5 CNDs, respectively. Values are means ± range (n=30). P was accepted as 0.001. *P < 0.05, **P < 0.01, ****P < 0.0001. In boxplots, center bars represent medians and expand to the first and third quartiles; whiskers extend to min/max data points.

Therefore, we quantified the PL intensity of the modified CNDs that are treated with glioblastoma (SJ-GBM2) cells with and without the presence of inhibitors. The PL intensities of images were calculated through ImageJ software, and the results were analyzed with One-

way Anova statistical technique. The SJ-GBM2 cells were treated in the same manner as the previous imaging study except with the addition of competitive inhibitors to the same cell media. The treatment of modified CNDs and inhibitor solutions did not change the morphology and viability of the cells **(Fig. S5)**. Firstly, the original 1:1 CNDs' PL intensity were affected the presence of both the ASCT2 and the LAT1 transporters' competitive molecules **(Fig. 8, B)**. Therefore, there is a possibility that the 1:1 CNDs are also prone to be up taken by both the ASCT2 and the LAT1 transporters. Furthermore, with the presence of the ASCT2 and the LAT1 transporter inhibitors, the PL intensity of the 1:3 CNDs also decreased **(Fig. 8, C)**. In other words, the 1:3 CNDs are prone to use both the ASCT2 and the LAT1 transporters to enter the cancer cells, so the presence of one of the competitive inhibitors lessened their uptake. For the case of the 1:5 CNDs, we observed complete inhibition of PL intensity with the presence of the LAT1 transporter inhibitors **(Fig. 8, D)**. Meanwhile, the presence of ASCT2 transporter inhibitors did not affect PL intensity of the 1:5 CNDs **(Fig. 8, D)**.

In addition, it has been well known that for passive endocytic cell uptake nanoparticles with positive charge are more preferred comparing to negatively charged particles. While, in active cell uptake routes the interactions of transporters' ligand binding site with particles

determines the cellular uptake rates.[39] It has been shown that after the doxorubicin conjugation all of the modified CNDs exhibited significant increase in the surface charge. From the previous statement, we can interpret that their cellular uptake rates via passive routes may be enhanced. On the other hand, our *in vitro bioimaging* studies suggest that superior cancer selective uptake and directly better anti-cancer efficacies of 1:3 CNDs and 1:3 CNDs-Dox nano systems are also highly linked with the interaction between the transporters' ligand binding site and the modified CNDs through active cellular uptake routes.

The majority of existing CDs in literature lack of studies about their cellular uptake mechanism.[40] Additionally, papers which discuss the cellular uptake of current CDs emphasize highly on the passive routes instead of active routes.[41,42] Therefore, this study provides elaborated information about not only the passive routes but also the active pathways.

To summarize, we hypothesized that possible cellular uptake mechanism of the 1:1, 1:3 and the 1:5 CNDs changed with the modifications of their surface structural groups. Especially, the 1:1 and the 1:3 CNDs tend to penetrate the cells through both ASCT2 and LAT1 transporters due to having surface functional groups such as primary amines, carboxylic groups, and alcohol groups that resemblance small amino acids. On the other hand, the 1:5

CNDs carry more N pyridinic groups (and lack -OH groups) on their surface which resemble to large amino acids and prefers the LAT1 pathway.

## 4. Conclusions

Here, we have successfully synthesized surface modified CNDs by changing the precursors' ratios. Our characterization results have shown that an increase in the amount of urea as a precursor also increments the amount of surface -$NH_2$ groups in addition to a decrease of -COOH groups. Modified CNDs meticulously characterized to assess their optical, size and morphology, surface functional groups and surface charge properties. We performed a carbodiimide coupling with doxorubicin to use these modified CNDs as nanocarriers. Due to the favorable surface charges, we were able to load more doxorubicin on 1:3 and 1:5 CNDs. Next, the CNDs-Dox conjugates were applied on 6 distinct cell lines for *in vitro* viability studies. Both the 3 and the 72 hours of treatments have shown that biocompatibility of the 1:3 and the 1:5 CNDs-Dox did not change compared to the 1:1 CNDs-Dox towards the non-tumor cell line. On the other hand, the 1:3 and the 1:5 CNDs-Dox conjugates performed significantly better anticancer efficacy against most of the cancer cells. Especially, the 1:3 CNDs-Dox conjugates performed improved anticancer efficacy for some cases compared to doxorubicin

standalone. We were able to introduce less doxorubicin but still acquire better anticancer efficacy with the CNDs-Dox conjugations. We hypothesized that having significant anticancer effects on some cancer cell lines but not all of them could be related to the possible cellular uptake mechanism of the modified CNDs. Hence, we performed Western blot studies on the cell lines that have been employed to measure the expression levels of two common cancer cell transporters: ASCT2 and LAT1. According to Western blotting, there is an alignment between the anti-cancer efficacy of CNDs-Dox conjugates and expression levels of ASCT2 and LAT1 transporters on the cell lines tested. Next, *in vitro* bioimaging studies were applied to further investigate the effects of surface functional groups on the cellular uptake of CNDs. Both the 1:3 and the1:5 CNDs were able to keep the selective cancer cellular uptake. In addition, they exhibit significantly higher PL intensities compared to the original 1:1 CNDs. Finally, we introduced five competitive ligands of ASCT2 and LAT1 into the CNDs bioimaging environment to assess changes in the PL intensity of the CNDs. PL intensities of both 1:1 and 1:3 CNDs were decreased with the presence of both ASCT2 and LAT1 transporter inhibitors. However, only LAT1 transporter inhibitors were able to significantly weaken the PL intensity of the 1:5 CNDs. Our studies suggest that possible cell uptake mechanism of 1:1

and 1:3 CNDs is linked to ASCT2 and LAT1 transporters. Consequently, 1:5 CNDs are prone to be taken up by LAT1 transporters of the cells. This study provides a chemical and biological foundations for understanding the effects of surface functional groups of nanocarriers to their cellular uptake mechanism. For future applications, this study opens a novel door for building personalized nanomedicine for specific cancer types by the effects of the surface functional groups.

## Author Contributions:

E.K.C designed and performed experiments, analyzed data, and wrote the paper; M.S and F.A.V helped with the *in vitro* studies. J.M.G assisted synthesis of CNDs; M.B. and A.T. performed XPS studies and build reaction scheme for the structure of CNDs; S.V. contributed to the revision of the manuscript; R.M.G. and R.M. L. supervised the experiments and edited the manuscript; All authors discussed the results and implications and commented on the manuscript at all stages.

## Conflicts of interest

There are no conflicts to declare.

## Acknowledgements

R. M. L. thanks the support from National Science Foundation under the grant 1809060 and 2041413. R.M.G. gratefully acknowledges the support of the BCURED Foundation, the Florida Department of Health Live Like Bella research grant 21L08 and the Mystic Force Foundation. Also, authors gratefully acknowledge the great support from University of Miami, USA.

## References

1. Wang, Y., Zhu, Y., Yu, S. & Jiang, C. Fluorescent carbon dots: rational synthesis, tunable optical properties and analytical applications. *RSC Adv* **7**, 4973–4989 (2017).

2. Issa, M. A. *et al.* Fluorescent recognition of Fe3+ in acidic environment by enhanced-quantum yield N-doped carbon dots: optimization of variables using central composite design. *Sci Rep* **10**, 11710–11710 (2020).

3. Li, L. & Dong, T. Correction: Photoluminescence tuning in carbon dots: surface passivation or/and functionalization, heteroatom doping. *Journal of materials chemistry. C, Materials for optical and electronic devices* **7**, 315–315 (2019).

4. Esfandiari, N. *et al.* Effect of carbonization degree of carbon dots on cytotoxicity and photo-induced toxicity to cells. *Heliyon* **5**, e02940–e02940 (2019).

5. Hassan, S. *et al.* Evolution and clinical translation of drug delivery nanomaterials. *Nano Today* **15**, 91–106 (2017).

6. Fenstermacher, D. A., Wenham, R. M., Rollison, D. E. & Dalton, W. S. Implementing personalized medicine in a cancer center. *The cancer journal (Sudbury, Mass.)* **17**, 528–536 (2011).

7. *Confirmation hearings on the nominations of Thomas Perrelli, nominee to be Associate Attorney General of the United States and Elena Kagan, nominee to be Solicitor General of the United States : hearing before the Committee on the Judiciary, United States Senate, One Hundred Eleventh Congress, first session, February 10, 2009.* (U.S. G.P.O., 2009).

8. Neal, J. W. *et al.* Erlotinib, cabozantinib, or erlotinib plus cabozantinib as second-line or third-line treatment of patients with EGFR wild-type advanced non-small-cell lung cancer (ECOG-ACRIN 1512): a randomised, controlled, open-label, multicentre, phase 2 trial. *The lancet oncology* **17**, 1661–1671 (2016).

9. Druker, B. J. *et al.* Five-Year Follow-up of Patients Receiving Imatinib for Chronic Myeloid Leukemia. *N Engl J Med* **355**, 2408–2417 (2006).

10. Liyanage, P. Y. *et al.* Carbon Nitride Dots: A Selective Bioimaging Nanomaterial. *Bioconjug Chem* **30**, 111–123 (2019).

11. Still, E. R. & Yuneva, M. O. Hopefully devoted to Q: targeting glutamine addiction in cancer. *Br J Cancer* **116**, 1375–1381 (2017).

12. Lopes, C., Pereira, C. & Medeiros, R. ASCT2 and LAT1 Contribution to the Hallmarks of Cancer: From a Molecular Perspective to Clinical Translation. *Cancers (Basel)* **13**, 203 (2021).

13. Halvorson, K. G. *et al.* A high-throughput in vitro drug screen in a genetically engineered mouse model of diffuse intrinsic pontine glioma identifies BMS-754807 as a promising therapeutic agent. *PLoS One* **10**, e0118926–e0118926 (2015).

14. Zhou, Y. *et al.* Photoluminescent Carbon Dots: A Mixture of Heterogeneous Fractions. *Chemphyschem* **19**, 2589–2597 (2018).

15. Kirbas Cilingir, E. *et al.* Metformin derived carbon dots: Highly biocompatible fluorescent nanomaterials as mitochondrial targeting and blood-brain barrier penetrating biomarkers. *J Colloid Interface Sci* **592**, 485–497 (2021).

16. Graham, R. M. *et al.* Resveratrol augments ER stress and the cytotoxic effects of glycolytic inhibition in neuroblastoma by downregulating Akt in a mechanism independent of SIRT1. *Exp Mol Med* **48**, e210–e210 (2016).

17. van Dam, B. *et al.* Excitation-Dependent Photoluminescence from Single-Carbon Dots. *Small* **13**, 1702098-n/a (2017).

18. Keenan J Mintz, Yiqun Zhou & Roger M Leblanc. Recent development of carbon quantum dots regarding their optical properties, photoluminescence mechanism, and core structure. *Nanoscale* **11**, 4634–4652 (2019).

19. Ţucureanu, V., Matei, A. & Avram, A. M. FTIR Spectroscopy for Carbon Family Study. *Crit Rev Anal Chem* **46**, 502–520 (2016).

20. Cao, X. *et al.* A facile microwave-assisted fabrication of fluorescent carbon nitride quantum dots and their application in the detection of mercury ions. *Spectrochim Acta A Mol Biomol Spectrosc* **151**, 875–880 (2015).

21. Lerf, A., He, H., Riedl, T., Forster, M. & Klinowski, J. 13C and 1H MAS NMR studies of graphite oxide and its chemically modified derivatives. *Solid State Ion* **101**, 857–862 (1997).

22. Kanwal, U. *et al.* Advances in nano-delivery systems for doxorubicin: an updated insight. *J Drug Target* **26**, 296–310 (2018).

23. Ferreira, B. C. L. B., Liyanage, P. Y. & Leblanc, R. M. Drug Loading of Anthracycline Antibiotics on Carbon Dots Using Circular Dichroism Spectrometry. *Analytical chemistry (Washington)* **93**, 14773–14777 (2021).

24. Yang, X. *et al.* Hyaluronic acid/EDC/NHS-crosslinked green electrospun silk fibroin nanofibrous scaffolds for tissue engineering. *RSC Adv* **6**, 9972–99728 (2016).

25. García Rubia, G. *et al.* pH-Dependent Adsorption Release of Doxorubicin on MamC-Biomimetic Magnetite Nanoparticles. *Langmuir* **34**, 13713–13724 (2018).

26. Bae, Y. H. & Park, K. Targeted drug delivery to tumors: Myths, reality and possibility. *Journal of controlled release* **153**, 198–205 (2011).

27. Graham, R. M. *et al.* Resveratrol augments ER stress and the cytotoxic effects of glycolytic inhibition in neuroblastoma by downregulating Akt in a mechanism independent of SIRT1. *Exp Mol Med* **48**, e210–e210 (2016).

28. Bjerke, L. *et al.* Histone H3.3. mutations drive pediatric glioblastoma through upregulation of MYCN. *Cancer Discov* **3**, 512–519 (2013).

29. TRENT, J. *et al.* Evidence for Rearrangement, Amplification, and Expression of c-myc in a Human Glioblastoma. *Proceedings of the National Academy of Sciences - PNAS* **83**, 470–473 (1986).

30. Tambay, V., Raymond, V.-A. & Bilodeau, M. MYC Rules: Leading Glutamine Metabolism toward a Distinct Cancer Cell Phenotype. *Cancers (Basel)* **13**, 4484 (2021).

31. Fuchs, B. C. & Bode, B. P. Amino acid transporters ASCT2 and LAT1 in cancer: Partners in crime? *Semin Cancer Biol* **15**, 254–266 (2005).

32. Pochini, L., Scalise, M., Galluccio, M. & Indiveri, C. Membrane transporters for the special amino acid glutamine: structure/function relationships and relevance to human health. *Front Chem* **2**, 61–61 (2014).

33. Zhang, J. *et al.* Review of the Correlation of LAT1 With Diseases: Mechanism and Treatment. *Front Chem* **8**, 564809–564809 (2020).

34. van Geldermalsen, M. *et al.* Benzylserine inhibits breast cancer cell growth by disrupting intracellular amino acid homeostasis and triggering amino acid response pathways. *BMC Cancer* **18**, 689–689 (2018).

35. van Geldermalsen, M. *et al.* ASCT2/SLC1A5 controls glutamine uptake and tumour growth in triple-negative basal-like breast cancer. *Oncogene* **35**, 3201–3208 (2016).

36. Schulte, M. L. *et al.* Pharmacological blockade of ASCT2-dependent glutamine transport leads to antitumor efficacy in preclinical models. *Nat Med* **24**, 194–202 (2018).

37. Cibrian, D. *et al.* Erratum: CD69 controls the uptake of L-tryptophan through LAT1-CD98 and AhR-dependent secretion of IL-22 in psoriasis. *Nat Immunol* **17**, 1235–1235 (2016).

38. Yan, R. *et al.* Mechanism of substrate transport and inhibition of the human LAT1-4F2hc amino acid transporter. *Cell Discov* **7**, 16–16 (2021).

39. Saadat, M. *et al.* Drug Targeting Strategies Based on Charge Dependent Uptake of Nanoparticles into Cancer Cells. *Journal of pharmacy & pharmaceutical sciences* **22**, 191–220 (2019).

40. Fu, C., Qian, K. & Fu, A. Arginine-modified carbon dots probe for live cell imaging and sensing by increasing cellular uptake efficiency. *Materials Science & Engineering C* **76**, 350–355 (2017).

41. Wei, Y., Jin, X., Kong, T., Zhang, W. & Zhu, B. The endocytic pathways of carbon dots in human adenoid cystic carcinoma cells. *Cell Prolif* **52**, e12586-n/a (2019).

42. Halder, A. *et al.* One-Pot Green Synthesis of Biocompatible Graphene Quantum Dots and Their Cell Uptake Studies. *ACS Appl Bio Mater* **1**, 452–461 (2018).